Swarthmore College
Works

Engineering Faculty Works | Engineering

12-1-1995

An Interferometric Technique For B/A Measurement

E. Carr Everbach
Swarthmore College, ceverba1@swarthmore.edu

R. E. Apfel

Follow this and additional works at: https://works.swarthmore.edu/fac-engineering

Part of the Engineering Commons

Let us know how access to these works benefits you

Recommended Citation
E. Carr Everbach and R. E. Apfel. (1995). "An Interferometric Technique For B/A Measurement". *Journal Of The Acoustical Society Of America*. Volume 98, Issue 6. 3428-3438. DOI: 10.1121/1.413794
https://works.swarthmore.edu/fac-engineering/64

This work is brought to you for free by Swarthmore College Libraries' Works. It has been accepted for inclusion in Engineering Faculty Works by an authorized administrator of Works. For more information, please contact myworks@swarthmore.edu.

An interferometric technique for B/A measurement

E. Carr Everbach[a)] and Robert E. Apfel
Yale Center for Acoustics, Yale University, 2159 Yale Station, New Haven, Connecticut 06520

(Received 5 April 1991; revised 1 May 1995; accepted 11 July 1995)

An isentropic phase method is described for measuring *in vitro* the acoustic nonlinearity parameter B/A of several aqueous buffers, protein solutions, lipid oils, and emulsions. The technique relies upon the use of an acoustic interferometer to measure the small changes in sound speed that accompany a rapid hydrostatic pressure change of between one and two atmospheres. Average accuracies of 0.85% are attainable with this method. © *1995 Acoustical Society of America.*

PACS numbers: 43.25.Ba, 43.80.Ev

INTRODUCTION

For more than 35 years, various methods for measuring the acoustic nonlinearity parameter B/A of a medium have been proposed.[1–4] The two most popular measurement techniques are the finite amplitude[5] and the thermodynamic methods,[6] which differ in that the finite amplitude method uses the distortion of the wave as it propagates as a measure of the B/A value of a material while the thermodynamic method relies upon changes in gross sound speed that accompany changes in ambient pressure and temperature. An important variation of the thermodynamic method is the isentropic phase method, in which sound speed is measured during a sufficiently rapid and smooth pressure change that the system is considered thermodynamically reversible.[7–11] This method has the advantage that detailed knowledge of the thermodynamic properties such as the heat capacity and coefficient of thermal expansion of the material is unnecessary. The precision with which B/A can be measured is about 10% for the finite amplitude method, 5% for the thermodynamic method, and 4% for the isentropic phase methods. A comprehensive review of these measurement techniques can be found in Ref. 12.

More recently, however, techniques with greater precision have been necessitated by the use of the acoustic nonlinearity parameter in predictive models of mixture composition[13–15] and nonlinear acoustic propagation in biological tissues.[16,17] Several investigators have developed techniques that can measure the B/A value of a material *in vitro* to an accuracy of within 1%, though each technique has its attendant advantages and disadvantages. These techniques employ variations of the isentropic method and are distinguished by the methods employed to measure the small changes in propagation time that occur with an adiabatic pressure change.[18,19] The method described in this paper has the advantage over similar methods[9] of being automated so that many thousands of independent measurements can be made on a particular sample in a reasonable time. Statistical procedures are then applied to the resulting data to determine both the best estimate of the material's true B/A value and a quantification of the error bounds on this estimate. Furthermore, this technique uses imposed hydrostatic pressure changes small enough to be potentially achievable using low-frequency acoustic "pump" waves.

I. MEASUREMENT SYSTEM

The apparatus was designed to measure the acoustic nonlinearity parameter B/A with an accuracy of 1% as a material is subjected to a maximum static pressure variation of less than 2 atm (gage pressure). A further design goal was that the material be subjected to no temperature excursions during measurement that might alter its chemical or physical properties.

The method presented here uses an acoustic interferometer to measure the very small changes in acoustic phase speed that occur when the pressure in the propagation medium is changed adiabatically. This change of sound speed for a given change of pressure is proportional to B/A through the relation[20]

$$\frac{B}{A}=2\rho_0 c_0\left(\frac{\partial c}{\partial p}\right)_s \approx 2\rho_0 c_0\left(\frac{\Delta c}{\Delta p}\right)_s, \tag{1}$$

where ρ_0 is the undisturbed density of the medium and Δc is the sound-speed change resulting from a pressure change Δp for which the entropy s is constant. The term in parentheses is typically on the order of 2×10^{-6} m/s/Pa for water and biological liquids. Since a pressure change of 1 atm would result in a change of sound speed of about 0.1 m/s for water at body temperature, to resolve this change sufficiently well to achieve 1% accuracy, it is necessary to measure changes in sound speed of 0.001 m/s, or a fractional change in sound speed of 6.7×10^{-7}.

We use a commercially available acoustic interferometer, the PLR-1000 from MicroUltrasonics, Inc. (Hampton, VA), which contains a microprocessor-controlled phase-locked-loop circuit to adjust the frequency of the source transducer so that a constant phase relationship is maintained at the receiving transducer as the gross sound speed in the medium changes. Since frequency counters are capable of excellent resolution (±1 Hz in 10 MHz is typical), the PLR-1000 can resolve changes in sound velocity to one part in 10^7. Small temperature fluctuations taking place during the measurement will change the sound speed in the material, however, and this effect is indistinguishable from the pressure-induced sound-speed changes we seek to measure.

[a)]Current address: Department of Engineering, Swarthmore College, Swarthmore, PA 19081.

Redistribution subject to ASA license or copyright; see http://acousticalsociety.org/content/terms. Download to IP: 130.58.65.20 On: Thu, 21 May 2015 16:02:08

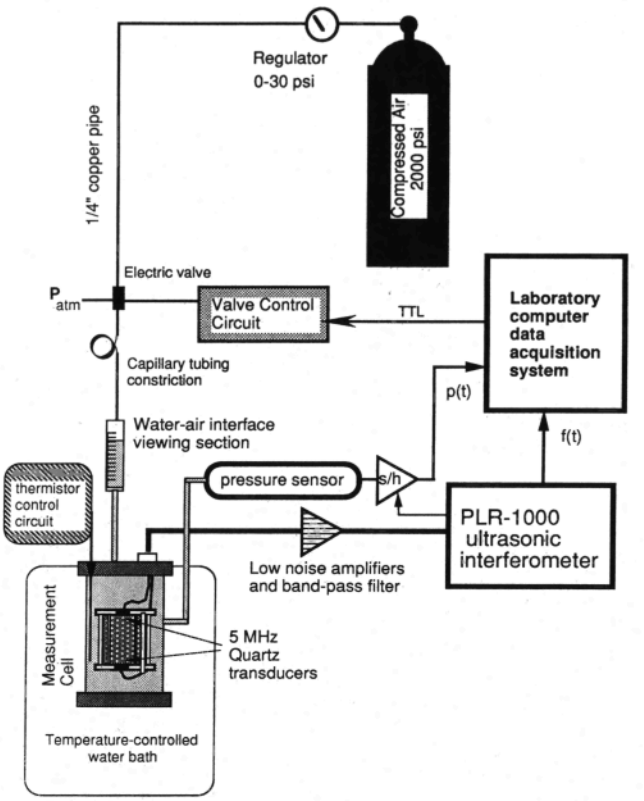

FIG. 1. Schematic description of B/A measurement apparatus.

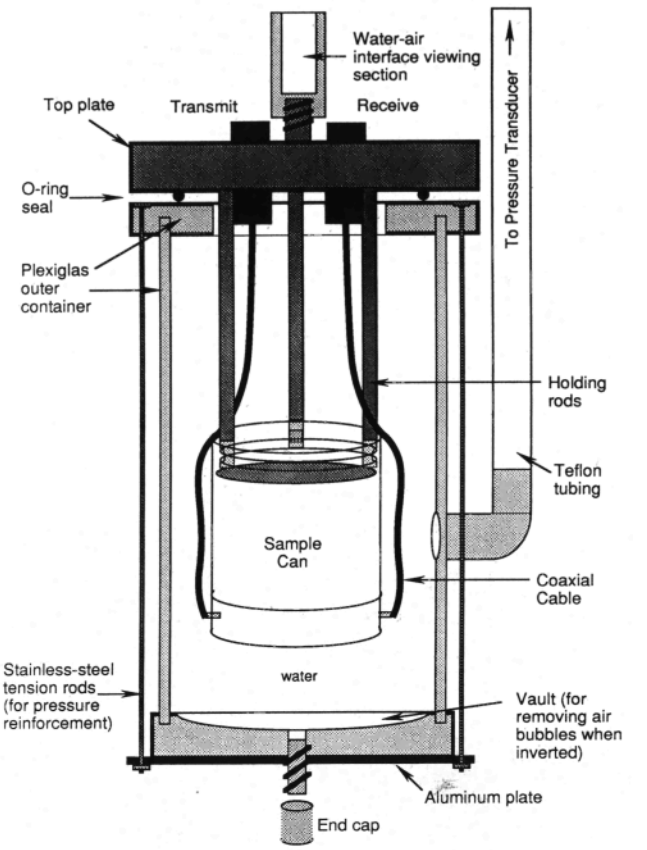

FIG. 2. Diagram of measurement cell (not to scale).

For instance, a change in temperature of 0.0024 °C will result in a change of sound speed in water of 0.001 m/s, which is the 1% resolution we seek to achieve. Using a Lauda/Brinkmann B-2/RC-3B temperature bath, we were able to control temperature in the sample material to about 0.001 °C for the duration of each measurement (3 s), as measured by a calibrated precision thermistor (Omega 44204). To overcome the effects of thermal and electrical noise, the automation and statistical processing outlined in the next section are applied to provide the best estimate of the true B/A value of the material.

Figure 1 is a block diagram of the measurement system. The measurement cell contains the sample material, maintains it at a constant temperature, and allows it to be pressurized. The pressure connection to the cell is made via a section of 1/4-in. (6.25-mm)-o.d. copper pipe that extends from the water–air interface viewing section to one end of a coil of stainless-steel capillary tubing. This tubing acts as a pressure constriction, slowing the equalization of the pressurized cell when it is vented to atmospheric pressure. The other end of the capillary tubing is connected to a section of copper pipe that passes through a valve to a pressure regulator. The valve is electrically activated, and can be opened or closed remotely by a computer-controlled circuit. When opened, this valve connects the cell to the pressure regulator, when closed, to atmospheric pressure. The regulator is maintained at approximately 185 kPa static pressure (1.85 atm), and is charged via a large tank of compressed air, as shown. The motion of the water–air interface in the acrylic viewing section mounted on the top plate of the cell provides a visualization of the cell's pressurization and depressurization.

A. Pressure measurement

In order to measure the instantaneous pressure in the cell as a function of time, an Omega PX800 pressure transducer mounted above the cell communicates with the cell via a short piece of Teflon® tubing. The pressure transducer provides a voltage that is proportional to the gage pressure in the cell with a linearity accuracy of less than 0.1% in the range of interest. The output voltage is sent to a "sample-and-hold" amplifier (s/h) that is triggered by the PLR-1000 to record simultaneously the instantaneous value of pressure and interferometer frequency. Two 5-MHz-center-frequency ultrasound transducers in the cell are linked electrically to the PLR-1000, which sends a 20-cycle tone burst to the transmitting transducer (producing an acoustic pressure amplitude of less than 1 atm in the medium) and receives an amplified and filtered signal from the other. The outputs of the interferometer and the sample-and-hold amplifier are sent to a laboratory computer system, which controls the electric valve and monitors both the changing sound speed in the sample (via the interferometer) and the changing pressure in the cell (via the pressure transducer).

Figure 2 shows the details of the measurement cell, which consists of two main elements: a "sample can," which holds the sample material and acoustic transducers, and the outer container, which acts as a pressure vessel to allow the contents of the can to be maintained above atmospheric pressure. The outer container is bolted to the stainless-steel top plate and sealed via O-rings. Most of the electrical and pressure connections are made through the top plate, which holds

Redistribution subject to ASA license or copyright; see http://acousticalsociety.org/content/terms. Download to IP: 130.58.65.20 On: Thu, 21 May 2015 16:02:08

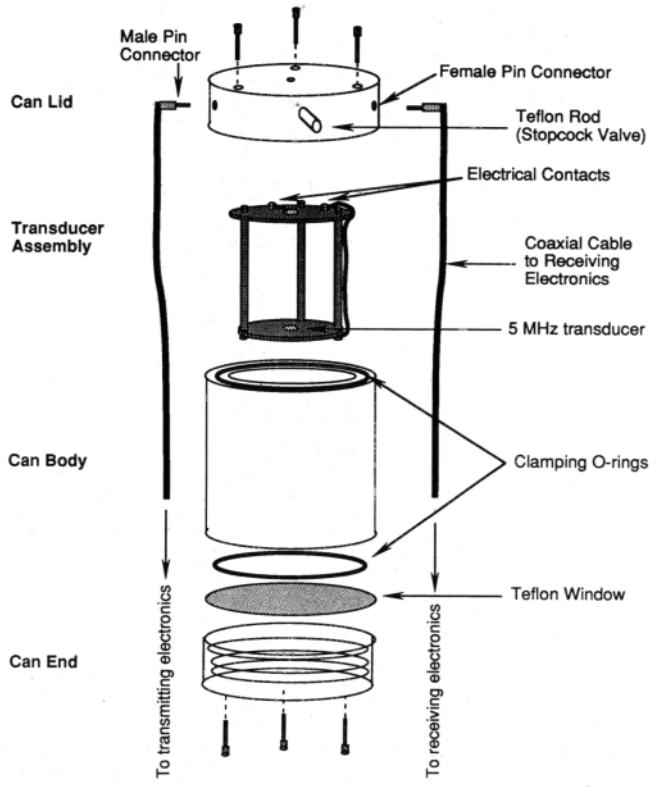

FIG. 3. Exploded view of sample can.

the sample can via three stainless-steel rods attached to the plate. In Fig. 2, dimensions are not shown because no dimension is critical to the functioning of the cell.

The transducer assembly which fits inside the sample can (Fig. 3) is a frame consisting of two parallel stainless-steel disks separated a distance of 3.14 cm by three 3.18-mm-diam stainless-steel spacing rods. The disks have diameters of 2.7 and 2.42 cm, respectively, and a thickness of 3.18 mm (the dimensions are not critical). At the center of each disk is mounted a 6.35-mm-diam unfocused transducer (gold-coated X-cut quartz for chemical unreactivity) that is resonant at 5 MHz. The facing transducer surfaces are both connected electrically to the assembly frame by conducting epoxy (Tecknit EMI Product 72-08116, Cranford, NJ), so that when the lid is bolted on and the electrical connections established, the assembly and the transducer faces will be electrically grounded. The back of each transducer is connected via a thin shielded wire to a small stainless-steel screw embedded in a piece of (nonconducting) Teflon® on the upper end of the assembly. In this way, the screws press against the small stainless-steel plates in the can lid when the lid is bolted on, establishing an electrical connection between each transducer surface in the assembly and a corresponding female pin connector in the can lid. The entire transducer assembly is held in the can via three Teflon® tabs that fit into shallow grooves in the walls of the can body. Unlike the measurement cells of other investigators,[10,21] the distance between the transducers does not change with applied hydrostatic pressure because the design of the sample can allows the transducer assembly to be pressurized equally on all sides.

In operation, the empty sample can is first filled with the sample to be measured, and then the transducer assembly is gently lowered into it. Because the can body is made of clear acrylic, it is possible to check visually for large bubbles that may have become trapped in the liquid between the transducers. The can lid is then bolted on, establishing electrical contact between the transducers and the female pin connectors, and large air bubbles are forced out of the exit hole in the lid. The stopcock valve in the exit hole is closed by rotating the Teflon® rod by 90°. The liquid to be measured is now completely contained within the can, which holds a volume of 20 ml of sample material.

The sample can is then inverted and clipped to the three holding rods of the outer container top plate, as shown in Fig. 2. The male pin connectors on the coaxial cables are connected to the female pin connectors in the sample can lid and to the bulkhead connectors in the container top plate. The acrylic outer container is bolted onto the top plate and the measurement cell is completely filled with 350 ml of clean, degassed water. The water acts to transmit pressure changes in the viewing section quickly and evenly to the material in the sample can via the Teflon® window and to the pressure transducer that monitors these changes. The entire measurement cell assembly is then lowered into the constant-temperature bath, and the pressure and electrical connections on the top plate are established.

B. Ultrasonic interferometer

The PLR-1000 pulsed phase-locked-loop acoustic interferometer has been specially modified to send 20-cycle acoustic tone bursts at 5-MHz center frequency (the device usually operates at 1 MHz or lower). These tone bursts are emitted at an adjustable pulse repetition frequency (PRF), usually about 750 Hz. The 5-MHz center frequency was chosen to provide a good compromise between two undesirable effects: the decrease in interferometer phase sensitivity at lower frequencies due to there being fewer wavelengths traversing the sample, and the increase in sample acoustic absorption that would attend higher-frequency transmission.

Before commencing a data run, the user specifies a number, dialed on a thumbwheel on the interferometer, which corresponds to a fixed time interval (in μs) after each tone burst is emitted from the transmitting transducer. The instant marking the conclusion of this time interval is called the "sample point" and is represented visually as a small deflection or "blip" on an oscilloscope screen connected to the PLR-1000. During a measurement, the instantaneous voltage of the receiving transducer at the sample point is recorded and compared with a fixed reference voltage by the microprocessor of the PLR-1000. If the two voltages are not equal, the PLR-1000 adjusts the transmitted center frequency of the succeeding tone burst by a small amount Δf, which has the effect of modifying the phase of the received wave and hence the instantaneous voltage at the sample point. This adjustment of the frequency continues until the sample point voltage and the reference voltage are equal (phase quadrature). At phase quadrature, there is, in effect, an integral number of half-wavelengths between the source and the receiving transducers. This relationship is maintained as the effective

Redistribution subject to ASA license or copyright; see http://acousticalsociety.org/content/terms. Download to IP: 130.58.65.20 On: Thu, 21 May 2015 16:02:08

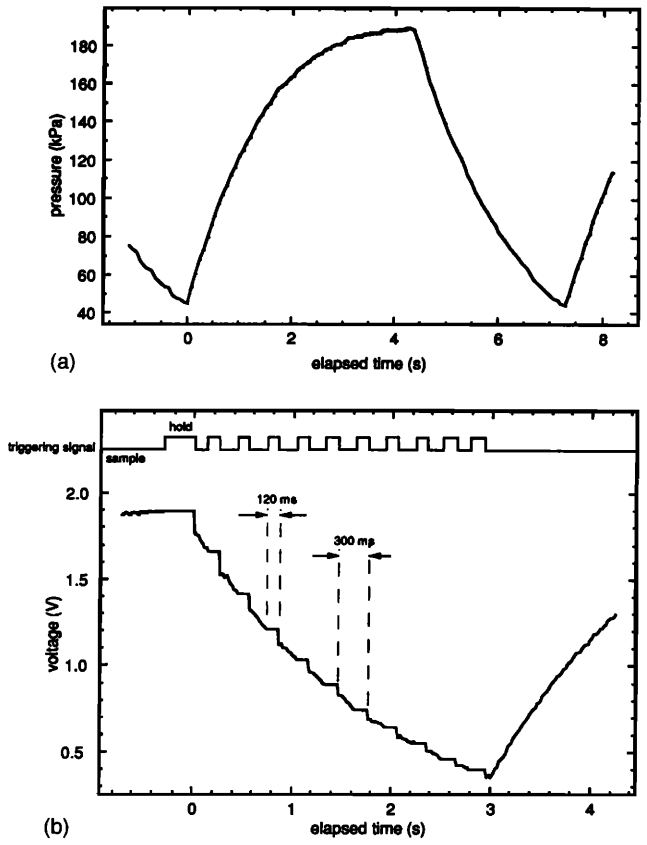

FIG. 4. (a) Pressure variations with time in measurement cell. (b) Triggering signal and corresponding output voltage of sample-and-hold amplifier as a function of time.

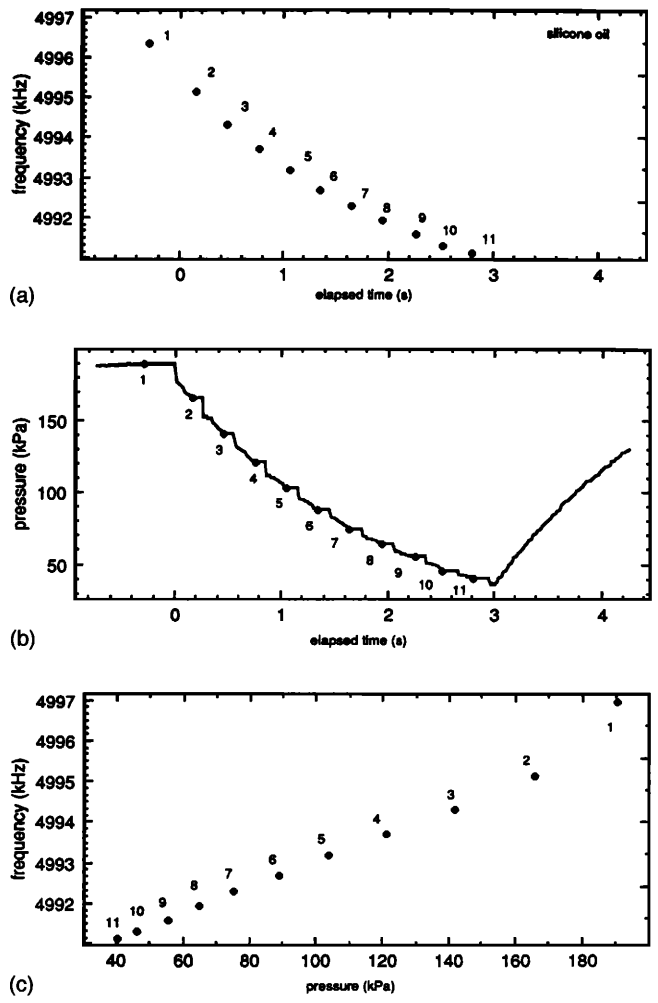

FIG. 5. (a) Interferometer frequency as a function of time. (b) Sample-and-hold amplifier output as a function of time converted to pressure units. (c) Interferometer frequency versus instantaneous pressure in measurement cell.

path length in the propagation medium changes because the PLR-1000 continuously adjusts the transmitting frequency to lock on to the phase quadrature condition.

The effective path length between the transducers changes because the sound velocity in the propagation medium changes an amount Δc due to a change in ambient pressure Δp in the medium. For a fixed transducer separation distance, the fractional change in interferometer frequency $\Delta f/f_0$ necessary to maintain quadrature is equal to the fractional change in sound speed $\Delta c/c_0$. Since $B/A=2\rho_0 c_0(\Delta c/\Delta p)$, the quantity $\Delta c/\Delta p$ equals $c_0\Delta f/f_0\Delta p$, and the following expression holds:

$$\frac{B}{A}=2\rho_0 c_0^2\frac{\Delta f}{f_0\Delta p}. \tag{2}$$

If we measure the slope $\Delta f/\Delta p$, therefore, it may be multiplied by the constant term $2\rho_0 c_0^2/f_0$ to yield B/A. In Eq. (2), f_0 is the interferometer frequency just prior to the pressure drop, e.g., 5 MHz. The values of ρ_0 and c_0 are measured separately using a sound velocity meter (Nusonics Inc. model 6080) and density meter (Mettler/Parr model DMA-40) both before and after the interferometric measurements.

The laboratory computer system controls the pressurization and depressurization of the measurement cell by remotely opening and closing the electric valve, resulting in the pressure versus time relationship shown in Fig. 4(a). The resulting changes in hydrostatic pressure $p(t)$ cause the sound speed, and hence the instantaneous frequency $f(t)$ of the interferometer, to change proportionately. The sample-and-hold amplifier is triggered by each display update of the PLR-1000, causing the pressure voltage at the instant of the display update to be held for 120 ms [Fig. 4(b)]. The computer data acquisition system records the pressure and the instantaneous interferometer frequency at the start of the 120-ms interval, and stores the values of the variables $p(t)$ and $f(t)$ at the particular times $t=t_1,t_2,\ldots,t_{10}$ for each pressure drop. Figure 5(a) and (b) shows typical frequency and pressure data, respectively, as a function of time for one pressure drop. Figure 5(c) is a plot of f_i vs p_i, and demonstrates that the slope $\Delta f/\Delta p$ can in principle be found from this measurement. Rather than calculating B/A independently for each pressure drop, however, we collect values of $\Delta f/\Delta p$ from many pressure drops and perform statistics on the ensemble, finally multiplying the mean value of $\Delta f/\Delta p$ by $2\rho_0 c_0^2/f_0$ to yield a value of B/A.

II. DATA PROCESSING

When a multiple of 250 pressure drops is achieved, the computer program performs a statistical analysis on the previous 250 consecutive data sets; this constitutes one data "block." The number 250 has been chosen to be large

Redistribution subject to ASA license or copyright; see http://acousticalsociety.org/content/terms. Download to IP: 130.58.65.20 On: Thu, 21 May 2015 16:02:08

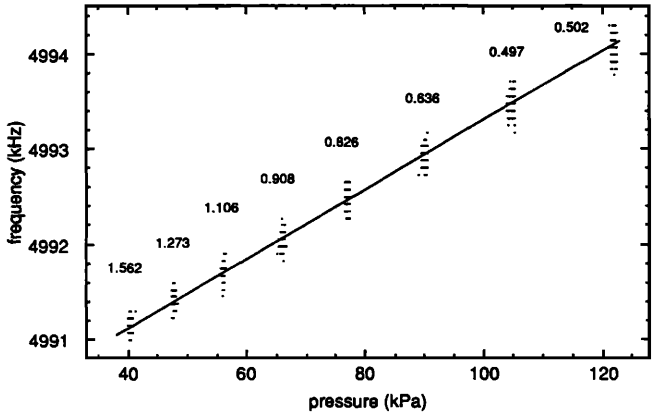

FIG. 6. Data block after normalization by average f-intercept showing weighting factors for points in each point cluster and weighted least-squares line through them. The slope of this line s is the best estimate of the slope of all data sets in the data block.

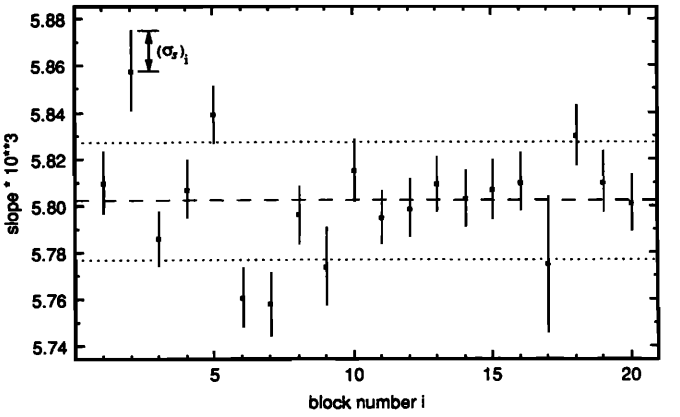

FIG. 7. Successive values of s. Error bars represent one standard deviation in s for each data block i, denoted by $(\sigma_s)_i$. The weighted average value $\bar{s}$ is represented by the dashed line, and one standard deviation of the data is represented by the dotted lines.

enough to provide a statistically significant sample while minimizing the computational overhead of storing larger amounts of data. For each of the 250 pressure drops, ten (p,f) points have been stored, along with the f intercept of the best-fit line through these points.

For the determination of B/A, we are interested in the best estimate of the slope $\Delta f/\Delta p$ of the data in a data block, and so we normalize all 250 ten-point data sets to the average f intercept of the block. Conceptually, this procedure is equivalent to shifting each set upward or downward until its intercept equals the average f intercept of the block. The slope of each ten-point set, however, is not altered. We then obtain an improved estimate of $\Delta f/\Delta p$ for the block by using a weighted least-squares algorithm in which the weighting functions include information about the standard deviations of each resulting point cluster, as shown in Fig. 6.

Following Bevington,[22] we compute the weighted least-squares line through the data of Fig. 6 with a weighting function equal to the inverse variances of f for the different point clusters. These weighting factors (the inverse variances) are displayed above each cluster for the example in Fig. 6. Each point in a given cluster shares the same weighting function as the other points in the cluster in the subsequent least-squares fit. By implementing this procedure, the equation of the best-fit straight line is more heavily weighted toward the denser point clusters, which, due to normalization of the intercepts, are the leftmost ones. The resulting computation yields a line of slope $s=\Delta f/\Delta p$, which is also plotted in Fig. 6. This slope of this line is taken as the best estimate of the slope of all the data in the block. An estimate of the measurement uncertainty or spread of the value for s is provided by the standard deviation of the slope, σ_s, which is calculated and stored along with s for each 250-point block.

In general, the measured values of $s=\Delta f/\Delta p$ are different from one data block to another (though the true value s_{true} is presumed to remain constant since it is proportional to B/A). Figure 7 is a typical plot of the value of the slopes s_i for many consecutive data blocks versus block number i. The error bars in this figure are equal to one standard deviation of the slope s_i based upon the data in the block; this standard deviation is denoted $(\sigma_s)_i$ for the ith block. Figure 7 shows that it is possible for the slope of one block to differ

TABLE I. Measurements of buffered aqueous solutions.

Material	T(°C)	ρ (kg/m^3)	c (m/s)	$B/A \pm \Delta(B/A)$	$\Delta(B/A)$ in %
Distilled water	20	998.2±0.1	1482.1±0.1	4.985±0.063	1.2
	30	995.7±0.1	1508.8±0.1	5.280±0.021	0.4
0.1-M MOPS	20	998.2±0.1	1482.1±0.1	5.013±0.044	0.9
	30	995.7±0.1	1509.4±0.1	5.252±0.021	0.4
Isotonic saline	20	1004.5±0.1	1494.1±0.2	5.540±0.032	0.6
	30	1001.7±0.1	1519.6±0.1	5.559±0.018	0.3
1% Surfynol® 465 surfactant in water	20	998.8±0.1	1482.2±0.1	4.934±0.039	0.8
	30	995.5±0.1	1509.3±0.1	5.217±0.036	0.7
1% SDS in 0.1-M MOPS	30	1000.9±0.1	1508.5±0.1	5.285±0.048	0.9
0.0015-M sodium azide in water	20	998.2±0.1	1482.1±0.1	4.996±0.043	0.9
	30	995.7±0.1	1508.8±0.1	5.298±0.031	0.6

Redistribution subject to ASA license or copyright; see http://acousticalsociety.org/content/terms. Download to IP: 130.58.65.20 On: Thu, 21 May 2015 16:02:08

TABLE II. Measurements of protein–water solutions of molecular weight MW, protein mass fraction Y_p, and volume fraction X_p.

Material	MW	Y_p	X_p	T(°C)	ρ (kg/m^3)	c (m/s)	$B/A \pm \Delta(B/A)$	$\Delta(B/A)$%
Bacitracin	1400	0.067	0.047	20	1014.3±0.1	1512.4±0.1	5.610±0.042	0.7
				30	1011.1±0.1	1535.8±0.1	5.674±0.051	0.9
		0.122	0.099	20	1032.2±0.1	1536.0±0.1	5.750±0.030	0.5
				30	1028.5±0.2	1555.3±0.2	5.960±0.042	0.7
Lysozyme	14 000	0.051	0.039	20	1013.7±0.1	1501.5±0.1	5.298±0.031	0.6
				30	1010.8±0.1	1526.0±0.1	5.788±0.047	0.8
		0.100	0.078	20	1029.0±0.1	1520.1±0.1	5.726±0.050	0.9
				30	1025.4±0.4	1543.5±0.2	6.393±0.062	1.0
β-lacto-globulin	35 000	0.072	0.052	20	1018.4±0.1	1511.0±0.1	5.564±0.043	0.8
				30	1015.4±0.1	1534.9±0.1	5.654±0.052	0.9
		0.120	0.086	20	1031.5±0.1	1530.6±0.1	5.577±0.049	0.9
				30	1028.6±0.2	1553.5±0.1	6.076±0.118	1.9
Hemoglobin	64 500	0.062	0.043	20	1015.5±0.1	1504.9±0.1	5.492±0.035	0.6
				30	1012.6±0.2	1529.1±0.1	5.743±0.026	0.5
		0.123	0.068	20	1025.1±0.1	1518.8±0.1	5.507±0.051	0.9
				30	1021.8±0.1	1541.7±0.1	5.765±0.055	1.0
BSA	68 000	0.091	0.074	20	1023.5±0.1	1507.3±0.1	5.521±0.139	2.5
				30	1020.5±0.1	1536.1±0.1	5.590±0.040	0.7
		0.141	0.113	20	1036.9±0.1	1522.0±0.1	5.819±0.041	0.7
				30	1033.9±0.1	1548.6±0.1	6.066±0.037	0.6
		0.157	0.133	20	1043.4±0.1	1529.6±0.1	5.946±0.031	0.5
				30	1040.4±0.1	1556.5±0.1	6.216±0.062	1.0
		0.298	0.232	20	1077.4±0.1	1572.0±0.1	6.839±0.055	0.8
				30	1074.0±0.1	1599.2±0.1	7.089±0.048	0.7
BSA and 1% SDS (native)		0.045	0.035	30	1005.8±0.1	1515.0±0.1	5.450±0.073	1.3
BSA and 1% SDS (denatured)		0.045	0.035	30	1009.1±0.1	1520.2±0.1	5.454±0.064	1.1
hexokinase	102 600	0.040	0.037	20	1017.5±0.1	1518.8±0.1	5.551±0.022	0.4
				30	1014.6±0.1	1542.7±0.1	5.763±0.086	1.5
γ-globulin	150 000	0.059	0.053	20	1014.7±0.1	1503.4±0.1	5.322±0.052	1.0
				30	1012.0±0.1	1528.7±0.1	5.623±0.030	0.5
		0.110	0.106	20	1030.2±0.1	1522.3±0.1	5.699±0.053	0.9
				30	1027.2±0.1	1545.8±0.1	5.788±0.036	0.6
urease	489 000	0.093	0.068	20	1032.1±0.4	1526.4±0.3	5.679±0.055	1.0
				30	1029.6±0.1	1547.5±0.1	5.875±0.040	0.7
gelatin (gelled)		0.061	0.050	20	1012.1±0.2	1499.8±0.1	5.284±0.032	0.6
				25	1013.3±0.1	1515.8±0.1	5.402±0.041	0.8
gelatin (ungelled)				25	1013.3±0.1	1515.8±0.1	5.396±0.009	0.2
				30	1008.9±0.1	1523.2±0.1	5.430±0.047	0.9

from the slope of a preceding one by more than the σ_s value of either block. These variations between successive data blocks are due to random fluctuations in s caused by electrical and thermal noise in the measurement apparatus. Thus s may be considered a random variable: $s = s_{\text{true}} + n$, where s_{true} is a constant and n represents the contribution of random noise. The effect of the noise on the values of s_i should be to increase the apparent spread of these values, but not to alter their mean value (i.e., n is presumed to be a zero-mean random variable). Therefore, according to the method of maximum likelihood, the best estimate of s_{true} that we can obtain from a data run is the weighted mean $\bar{s}$ of all the s_i in the data run. This weighted mean is given by Bevington as

$$\bar{s} = \sum_{i=1}^{n} \frac{s_i}{(\sigma_s^2)_i} \Bigg/ \sum_{i=1}^{n} \frac{1}{(\sigma_s^2)_i}, \tag{3}$$

where, as before, the weighting function is just the inverse

Redistribution subject to ASA license or copyright; see http://acousticalsociety.org/content/terms. Download to IP: 130.58.65.20 On: Thu, 21 May 2015 16:02:08

TABLE III. Measurements of lipid oils and fat.

Material	T(°C)	ρ (kg/m^3)	c (m/s)	$B/A \pm \Delta(B/A)$	$\Delta(B/A)$ in %
Corn oil	20	919.8±0.1	1469.1±0.2	10.666±0.074	0.7
	30	913.1±0.1	1437.0±0.1	10.574±0.026	0.2
Castor oil	20	961.0±0.1	1515.9±0.2	11.270±0.044	0.4
	30	954.1±0.2	1492.2±0.1	11.006±0.051	0.5
Olive oil	20	913.0±0.1	1463.8±0.1	11.136±0.042	0.4
	30	906.1±0.2	1435.3±0.2	11.066±0.641	5.8
Peanut oil	20	914.5±0.1	1465.7±0.1	10.911±0.065	0.6
	30	907.7±0.1	1436.0±0.1	10.680±0.038	0.4
Safflower oil	20	921.8±0.1	1470.0±0.2	11.610±0.102	0.9
	30	915.0±0.1	1437.9±0.1	11.161±0.083	0.7
Cod liver oil	20	926.1±0.1	1473.8±0.1	10.958±0.022	0.2
	30	919.2±0.2	1442.7±0.2	10.867±0.029	0.3
Tung oil	20	939.6±0.1	1507.1±0.1	11.278±0.031	0.3
	30	932.8±0.1	1473.6±0.1	11.064±0.041	0.4
Lamp oil	20	804.0±0.1	1345.0±0.1	11.156±0.053	0.5
	30	797.0±0.2	1309.2±0.2	10.918±0.104	1.0
Mineral oil	20	858.1±0.1	1441.8±0.2	11.331±0.020	0.2
	30	851.7±0.1	1409.5±0.1	11.497±0.038	0.3
Pump oil	20	875.8±0.1	1470.0±0.1	11.791±0.026	0.2
	30	869.4±0.1	1436.1±0.1	11.451±0.018	0.2
Silicone oil	20	971.1±0.2	1002.5±0.1	11.381±0.052	0.5
	30	961.8±0.1	977.7±0.1	11.461±0.017	0.1
Chicken fat	30	906.5±0.1	1437.0±1.0	11.270±0.090	0.8

variance of the slope for each data block. As an example, this weighted mean has been calculated for the data shown in Fig. 7, and is represented in the figure by a horizontal dashed line.

A conservative estimate of the uncertainty for $\bar{s}$ is given by a descriptor of the data spread: the standard deviation σ of the data, which in Fig. 7 has been plotted as dotted lines. The overall experimental uncertainty in the B/A value of the material, taking into account the uncertainties of all measured quantities, may therefore be found by rewriting Eq. (2) as

$$\frac{B}{A}=\frac{2}{f_0}\rho c^2 s, \tag{4}$$

where each of the experimentally determined quantities on the right-hand side contains some measurement uncertainty:

$$\rho=\rho_0\pm\Delta\rho, \quad c=c_0\pm\Delta c, \quad s=\bar{s}\pm\sigma.$$

Note that $\Delta\rho$ and Δc are not standard deviations based upon many measurements, but are the absolute accuracies of the instruments that were used to measure ρ_0, and c_0, respectively. The best estimate of B/A is given by considering only the mean quantities:

$$\frac{B}{A}=\frac{2}{f_0}\rho_0 c_0^2\bar{s}. \tag{5}$$

The most conservative estimate of the uncertainty in B/A, call it $\Delta(B/A)$, is provided by taking the magnitude of the extreme excursions of each variable in Eq. (4), viz.,

$$\Delta\left(\frac{B}{A}\right)=\left|\frac{2}{f_0}(\rho_0+\Delta\rho)(c_0+\Delta c)^2(\bar{s}+\sigma)-\frac{B}{A}\right|, \tag{6}$$

where B/A is given by Eq. (5). The B/A values for materials considered in this study are reported as $B/A\pm\Delta(B/A)$, where B/A is given by Eq. (5) and $\Delta(B/A)$ by Eq. (6). $\Delta(B/A)$ is also listed as a percentage of B/A.

Several papers have suggested both transmission[23,24] and reflection[25] techniques by which B/A may be imaged. Rapid pressurization/depressurization of the propagation material is necessary to measure $\partial c/\partial p$ isentropically to determine B/A. In several B/A imaging techniques, this pressure change is accomplished by the simultaneous propagation of a large-amplitude low-frequency acoustic wave (a so-called "pump" wave) and a low-amplitude, high-frequency interrogating wave (the "probe" wave) whose subsequent phase modulation by the pump wave supplies a measure of $\partial c/\partial p$. In principle, it should be possible to extend the measurement technique described here to application in an imaging system. From a knowledge of the change in tone-burst center frequency Δf with pump wave pressure amplitude Δp, B/A could be measured at different spatial positions by moving the point of intersection of the pump wave and the interferometer probe wave. Techniques involving crossed probe and pump waves have been suggested previously[26] but none has made use of the high resolution achievable with an acoustic interferometer.

Redistribution subject to ASA license or copyright; see http://acousticalsociety.org/content/terms. Download to IP: 130.58.65.20 On: Thu, 21 May 2015 16:02:08

TABLE IV. Composition of phantoms.

Phantom	Volume fractions	Material
1	0.800	water+surfactant
	0.200	mineral oil
2	0.900	water+surfactant
	0.100	mineral oil
3	0.700	water+surfactant
	0.300	mineral oil
4	0.500	water+surfactant
	0.500	mineral oil
5	0.900	water+surfactant
	0.100	silicone oil
6	0.950	water+surfactant
	0.050	silicone oil
7	0.813	0.1-M MOPS
	0.100	mineral oil
	0.087	BSA
8	0.842	0.1-M MOPS
	0.083	silicone oil
	0.075	BSA
9	0.800	0.1-M MOPS
"Liverlike" phantom	0.050	castor oil
	0.150	BSA
10	0.420	0.1-M MOPS
"Breastfatlike" phantom	0.550	castor oil
	0.030	BSA

III. PROCEDURES AND RESULTS

In this section we present the results of measurements made on various aqueous buffered solutions, protein solutions, lipid suspensions, and pure lipid oils using the measurement system described above. We also constructed protein–water–oil emulsions to act as tissue-mimicking phantoms for use in comparing various mixture methodologies.[15]

A. Buffered aqueous solutions

Several types of additives, dissolved in the water, can help control the form of mixtures of water, protein, and fat used as tissue-mimicking phantoms. Table I lists the measured values of density, sound speed, and B/A for various buffered solutions, along with the percent accuracy in B/A as dermined from Eq. (6). The distilled water was de-ionized and filtered to 0.2 μm and possessed an electrical resistance of approximately 17.1 MΩ/cm. MOPS is a biological buffering agent designed to maintain a solution in the range of physiological pH values 6.5–7.9, and was purchased in crystalline form from Sigma Chemical Company (product No. M-1254). A 0.1-M (molar) solution of MOPS in water was found to improve protein solubility in all protein concentrations considered in this study. Isotonic saline consists of 153-mM sodium chloride and 10-mM MOPS, and possesses a pH of 7.4. Surfynol® 465 is a commercially available water-soluble surfactant manufactured by Air Products and Chemicals, Inc. (Allentown, PA). A 1% (by volume) solution of this surfactant was effective in stabilizing micron-sized droplets of mineral oil in water, as described below. SDS (sodium dodecyl sulfate) was used in this investigation as a protein-denaturing agent. 1.5-mM sodium azide, an antibiotic, was found to be effective in preventing the growth of bacteria in the mixtures.

B. Protein solutions

Table II lists measured data on protein–water solutions. These proteins were selected because absorption and MRI (magnetic resonance imaging) data were available for them[27,28] and because they span a large range in molecular weight (MW). All globular proteins were obtained in concentrated form from Sigma Chemical Company and were dissolved in the 0.1-M MOPS buffer solution described above. Knox® unflavored gelatin was obtained at a local supermarket and dissolved in distilled water. The mass fraction Y_p and volume fraction X_p of each protein solution were determined by differential weighing of a specified volume of solution before and after evaporation.[29]

The maximum protein concentrations achieved in this study were limited by the cost of the crystalline concentrate and the fluid volume required by the apparatus (20 ml). In the case of BSA, an inexpensive and plentiful protein, the maximum measurable concentration was limited by the inherent acoustic absorption of the solution, which increases with increasing protein concentration. The measured parameters of a protein solution (BSA and SDS) before and after irreversible denaturization (by heat) are included in Table II. Since the molecular structure changes drastically when a protein is denatured (all but the primary structure of the protein is removed), it is surprising that the measured parameters change so little. Similarly, the bulk properties of gelatin were investigated as the gel cooled and set (gelling is a function of both temperature and time). We were interested in determining whether the reversible cross linking of the protein molecules resulted in a measurable change in the B/A value of gelatin. Table II shows that the results are similar to the case of the irreversible denaturization of BSA: In both cases a negligible change in the measured parameters occurred.

C. Lipid oils and fats

Lipid oils possess no vesicle structure but share many characteristics with the complex fats found in animal tissues. They are inexpensive and available in a pure form so that concentrations of 100% oil could be measured (as opposed to the relatively low concentrations of lipid concentrate which may be suspended in water). Table III lists B/A measurements of various plant oils, fish and animal oils, petroleum-derived oils, and synthetic oils using the isentropic phase method described above. We have also included measurements made on chicken fat for comparison with the lipid-oil data. Chicken fat was acquired by boiling chicken skin in water, skimming off the resulting oily layer, and filtering it to

Redistribution subject to ASA license or copyright; see http://acousticalsociety.org/content/terms. Download to IP: 130.58.65.20 On: Thu, 21 May 2015 16:02:08

TABLE V. Measurements on finely mixed phantoms.

Phantom	T(°C)	ρ (kg/m^3)	c (m/s)	$B/A \pm \Delta(B/A)$	$\Delta(B/A)$ in %
1	20	978.4±1.0	1475.0±1.0	6.926±0.066	1.0
	30	968.7±1.0	1484.0±1.0	7.299±0.056	0.8
2	20	977.3±1.0	1484.0±1.0	5.912±0.059	1.0
	30	983.1±1.0	1495.0±1.0	6.306±0.042	0.6
3	20	961.0±2.0	1460.0±2.0	7.524±0.071	0.9
	30	942.0±5.0	1471.0±2.0	8.062±0.089	1.1
4	20	913.0±5.0	1450.0±3.0	8.993±0.113	1.2
	30	922.0±5.0	1439.0±3.0	9.517±0.106	1.1
5	20	996.4±0.1	1385.2±0.1	9.036±0.047	0.5
	30	993.1±0.1	1395.7±0.1	9.264±0.098	1.1
6	20	997.2±0.1	1431.8±0.1	7.291±0.027	0.4
	30	994.3±0.1	1448.5±0.1	8.084±0.021	0.3
7	20	937.0±2.0	1567.0±2.0	6.654±0.121	1.8
	30	934.0±1.5	1595.0±2.0	6.907±0.100	1.4
8	20	1033.8±0.1	1431.8±0.1	9.031±0.074	0.8
	30	1021.3±0.2	1437.2±0.2	9.514±0.069	0.7
9	20	1043.5±1.0	1569.4±1.0	6.814±0.099	1.4
	30	1049.0±1.0	1552.0±1.0	6.741±0.078	1.2
10	20	984.2±1.0	1511.8±1.0	9.010±0.133	1.5
	30	992.2±1.0	1498.0±1.0	8.915±0.181	2.0

obtain a clear, yellow liquid. Although this liquid may contain proteins and other components, its measured properties suggest that it is composed largely of fat.

The lipid oils all appear to possess densities and sound speeds lower than that of water, and B/A values more than twice that of water. The lipid oil data also appear to resemble those for the more complex (and poorly characterized) fats present in chicken fat. These similarities support the use of the better-characterized lipid oils as an appropriate substitute for fat in experiments designed to test theories which use fat as a composition indicator.

D. Phantoms

In order to compare the efficacy of various mixture laws,[10,13] mixtures of some of the materials listed in the previous sections were made and their density, sound speed, and B/A values measured. A mixture whose component properties and relative volume fractions are known is often referred to as a phantom, especially if the mixture composition mirrors that of whole tissue. A description of the composition of each phantom is given in Table IV.

The phantoms made for this investigation were simple emulsions of lipid oils in an aqueous solution. The aqueous solutions consisted of distilled water (phantoms 1–6), or 0.1-M MOPS buffer with a dissolved protein, BSA (phantoms 7–10). In phantoms 1–4, a 1% (by volume) concentration of Surfynol® 465 surfactant was dissolved in the distilled water prior to the addition of the mineral oil. This surfactant helped to prevent oil-droplet coalescence, but was not required in the phantoms containing BSA since this protein has its own surfactantlike properties. Micron-sized oil droplets were produced in these emulsions by sonicating the

TABLE VI. Measurements on coarsely mixed phantoms.

Phantom	T(°C)	ρ (kg/m^3)	c (m/s)	$B/A \pm \Delta(B/A)$	$\Delta(B/A)$ in %
1	20	978.4±1.0	1475.0±1.0	6.615±0.052	0.8
	30	968.7±1.0	1485.0±1.0	7.017±0.068	1.0
2	20	977.3±1.0	1485.0±1.0	5.821±0.073	1.3
	30	983.1±1.0	1499.0±1.0	6.180±0.041	0.7
3	20	961.0±2.0	1465.0±2.0	7.333±0.089	1.2
	30	942.0±5.0	1479.0±2.0	7.751±0.060	0.8
4	20	913.0±5.0	1458.0±3.0	8.684±0.103	1.2
	30	922.0±5.0	1459.0±3.0	9.212±0.088	1.0
7	20	937.0±2.0	1594.0±2.0	6.676±0.126	1.9
	30	934.0±1.5	1628.0±2.0	6.980±0.120	1.7

Redistribution subject to ASA license or copyright; see http://acousticalsociety.org/content/terms. Download to IP: 130.58.65.20 On: Thu, 21 May 2015 16:02:08

mixture with a Heat Systems-Ultrasonics, Inc. model W350 Cell Disrupter at high power for about 10 min, followed by degassing under vacuum to remove bubbles from the emulsion.

The phantoms after sonication, contained oil droplets ranging in size from less than 1 to 30 μm. Although negligible coalescence of the droplets takes place over periods of 12 h or more, buoyancy forces acting on the individual droplets gradually cause them to rise against gravity. This effect, known as "creaming" (in the case of oils) or "sedimentation" (in the case of particles), results over time in a separating of the emulsion into a concentrated layer of many oil droplets and a layer of mostly water (or protein solution). An emulsion in a gravitational field will cream or sediment at a rate given by[30]

$$u=\frac{2gr^2(\rho_1-\rho_2)}{9\eta}, \tag{7}$$

where r is the mean droplet radius, η is the bulk viscosity of the continuous phase (e.g., η for water $\approx$0.01 P), g is the local gravitational acceleration, and the subscripts 1 and 2 refer to the droplet and host properties, respectively. For our emulsions, the creaming rate was approximately 3.2 μm/s, and since the sample can in our measurement cell is approximately 3 cm tall, full separation in the can was expected to occur in approximately 2.6 h. This time scale was verified by direct observation of the phantom in the (transparent) measuring cell. Any differences between data collected on a newly sonicated emulsion and data collected several hours later therefore would be expected to result from the change from a fine mixture to a layered one. As discussed elsewhere,[15] these differences have implications for the comparison of the mixture laws of Apfel,[13] which are developed for fine mixtures, and those of Sehgal *et al.*,[10] which apply to mixtures with layered components (i.e., "coarse" mixtures).

Three of the phantoms were not sonicated. Phantoms 5, 6, and 8 were dilutions of a commercially available silicone-oil emulsion, SM2162 (General Electric Company), which is composed of water, GE Silicone Oil SF96 (350), and a proprietary surfactant. Because the silicone-oil droplets in this emulsion are nanometer sized (produced via a proprietary preparation process), Brownian motion is sufficient to keep the droplets from rising. The emulsion is thus permanently homogenized and does not cream.

The maximum oil and protein concentrations we could measure were limited by the acoustic attenuation of the mixture. Since an acoustic impedance mismatch exists between the droplet material and the continuous phase, isotropic scattering of acoustic energy could occur even for droplets much smaller than an acoustic wavelength. Relaxation processes originating at the interface between the two phases, especially differential viscosity, may also contribute to acoustic absorption.

E. Finely mixed emulsions

Table V lists measurements made on the phantoms in Table IV soon after the mixture was made. In all cases, the relative mixing of the oil and water components was uniform on the scale of an acoustic wavelength (300 μm) during the measurement period.

F. Coarsely mixed emulsions

Table VI lists measurements made on phantoms under the same conditions as those of Table V, but after at least 6 h had elapsed. In the case of phantoms with oil droplets of radius 1–30 μm (phantoms 1, 2, 3, 4, and 7), this time period was sufficient for the emulsion to have creamed completely. Thus most of the oil component was located in a region near the upper end of the measurement cell and most of the water (or protein and water) filled the remainder of the cell. An examination of differences in the measured B/A values of a phantom as the emulsion creams (Tables V and VI) may help yield insight into the role that larger-scale structure plays in determining a mixture's nonlinear acoustic properties.[29]

IV. CONCLUSION

The apparatus and procedures described here have been applied successfully to the measurement of the acoustic nonlinearity parameter B/A for a range of organic and aqueous solutions. The technique provides average measurement accuracies of 0.85% for the materials measured in this study and does not subject the measured sample to wide extremes of temperature and pressure. While not suitable for direct application to *in vivo* measurement of biological tissues, the method demonstrates the feasibility of accurate B/A measurement using small induced pressure variations.

ACKNOWLEDGMENTS

This work was supported in part by the U.S. Office of Naval Research and by the National Institutes of Health through Grants No. 2-R01-GM30419-04 and No. R04-GM30419.

[1] R. T. Beyer, "Parameter of Nonlinearity in Fluids," J. Acoust. Soc. Am. **32**, 719–721 (1960).

[2] W. K. Law, L. A. Frizzell, and F. Dunn, "Determination of the nonlinearity parameter B/A of biological media," Ultrasound Med. Biol. **11**(2), 307–318 (1985).

[3] H. A. Kashkooli, P. J. Dolan, Jr., and C. W. Smith, "Measurement of the acoustic nonlinearity parameter in water, methanol, liquid nitrogen, and liquid helium-II by two different methods: a comparison," J. Acoust. Soc. Am. **82**, 2086–2089 (1987).

[4] L. Adler and E. A. Hiedmann, "Determination of the nonlinearity parameter B/A for water and m-xylene," J. Acoust. Soc. Am. **34**, 410–412 (1962).

[5] W. N. Cobb, "Measurement of the Acoustic Nonlinearity Parameter of Biological Media," Ph.D. dissertation, Yale University, 1982.

[6] W. K. Law, L. A. Frizzell, and F. Dunn, "Comparison of thermodynamic and finite amplitude methods of B/A measurement in biological materials," J. Acoust. Soc. Am. **74**, 1295–1297 (1983).

[7] C. Kammoun, J. Emery, and P. Alias, "Determination of the acoustic parameter of nonlinearity in liquids at very low pressure," in the Seventh Intern. Symp. on Nonlinear Acoust., Virginia Polytechnic Inst. and State Univ., 1976, pp. 146–149.

[8] J. Emery, S. Gasse, and C. Dugué, "Coefficient de Nonlinearité Acoustique dans les Melanges Eau-Methanol et Eau-Ethanol," J. Phys. **11**(40), 231–234 (1979).

[9] Z. Zhu, M. S. Roos, W. N. Cobb, and K. Jensen, "Determination of the acoustic nonlinearity parameter B/A from phase measurements," J. Acoust. Soc. Am. **74**, 1518–1521 (1983).

[10] C. M. Sehgal, R. C. Bahn, and J. F. Greenleaf, "Measurement of the

Redistribution subject to ASA license or copyright; see http://acousticalsociety.org/content/terms. Download to IP: 130.58.65.20 On: Thu, 21 May 2015 16:02:08

acoustic nonlinearity parameter B/A in human tissues by a thermodynamic method," J. Acoust. Soc. Am. **76**, 1023–1029 (1984).

[11] X. Gong, Z. Zhu, T. Shi, and J. Huang, "Determination of the acoustic nonlinearity parameter in biological media using FAIS and ITD methods," J. Acoust. Soc. Am. **86**, 1–5 (1989).

[12] L. Bjørnø and P. A. Lewin, "Measurement of Nonlinear Acoustic Parameters in Tissue," in *Tissue Characterization with Ultrasound*, edited by J. F. Greenleaf (CRC, Boca Raton, FL, 1986), Chap. 6.

[13] R. E. Apfel, "Prediction of tissue composition from ultrasonic measurements and mixture rules," J. Acoust. Soc. Am. **79**, 148–152 (1986).

[14] C. M. Sehgal, G. M. Brown, R. C. Bahn, and J. F. Greenleaf, "Measurement and use of acoustic nonlinearity and sound speed to estimate composition of excised livers," Ultrasound Med. Biol. **12**(11), 865–874 (1986).

[15] P. Jiang, E. C. Everbach, and R. E. Apfel, "Applications of mixture laws for predicting the compositions of tissue phantoms," Ultrasound Med. Biol. **17**(8), 829–838 (1991).

[16] T. Christopher, "Modeling the Dornier HM3 lithotripter," J. Acoust. Soc. Am. **96**, 3088–3095 (1994).

[17] M. Grünewald and H. Koch, "Modelling of shock wave propagation in soft tissue," 13th International Congress on Acoustics, Belgrade, Yugoslavia, August 1989.

[18] J. Zhang and F. Dunn, "A small volume thermodynamic system for B/A measurement," J. Acoust. Soc. Am. **89**, 73–79 (1991).

[19] A. P. Sarvazyan, T. V. Chalikian, and F. Dunn, "Acoustic nonlinearity parameter B/A of aqueous solutions of some amino acids and proteins," J. Acoust. Soc. Am. **88**, 1555–1561 (1990).

[20] R. T. Beyer and S. V. Letcher, *Physical Ultrasonics*, Pure & Appl. Physics Ser. (Academic, New York, 1969).

[21] W. K. Law, "Measurement of the Nonlinearity Parameter B/A in Biological Materials using the Finite Amplitude and Thermodynamic Method," Ph.D. dissertation, University of Illinois at Urbana-Champaign, 1984.

[22] Philip R. Bevington, *Data Reduction and Error Analysis for the Physical Sciences* (McGraw-Hill, New York, 1969).

[23] N. Ichida, T. Sato, and M. Linzer, "Imaging the nonlinear ultrasonic parameter of a medium," Ultrason. Imag. **5**, 295–299 (1983).

[24] N. Ichida, T. Sato, A. Fukushima, H. Ishikawa, H. Miwa, K. Murakami, and Y. Igarashi, "Nonlinear Parameter Tomography by using pump waves," 10th International Symp. on Nonlinear Acoust., Kobe, Japan, 1984, pp. 227–232.

[25] C. A. Cain, "Ultrasonic reflection mode imaging of the nonlinear parameter B/A: I. A theoretical basis," J. Acoust. Soc. Am. **80**, 28–32 (1986).

[26] N. Ichida, T. Sato, H. Miwa, and K. Murakami, "Real-time nonlinear parameter tomography using impulsive pumping waves," IEEE Trans. Sonics Ultrason. **SU-31**(6), 635–641 (1984).

[27] F. W. Kremkau and R. W. Cowgill, "The role of molecular weight and structure in the absorption of ultrasound by proteins," in *Proceedings of the IEEE Ultrasonics Symposium* (IEEE, New York, 1984), pp. 696–698.

[28] F. W. Kremkau, "Solvent interactions and biomolecular absorption," Am. Inst. Ultrasound Med. 8–11 October, 113 (1985).

[29] E. C. Everbach, "Tissue composition determination via measurement of the acoustic nonlinearity parameter B/A," Ph.D. dissertation, Yale University, New Haven, CT, 1989.

[30] P. A. Sanders, *Handbook of Aerosol Technology* (Reinhold, New York, 1979), 2nd ed., p. 282.

Redistribution subject to ASA license or copyright; see http://acousticalsociety.org/content/terms. Download to IP: 130.58.65.20 On: Thu, 21 May 2015 16:02:08